

# Photoionization of Nanosized Aerosol Gold Agglomerates and Their Deposition To Form Nanoscale Islands on Substrates

Jeong Hoon Byeon and Jeffrey T. Roberts\*

Department of Chemistry, Purdue University, West Lafayette, Indiana 47907, United States

**ABSTRACT:** Positively charged gold nanoparticles can be produced in the aerosol state by ultraviolet irradiation of aerosols at wavelengths above the gold ionization energy. Spark-discharge-generated aerosol gold nanoparticles were mobility-classified, neutralized, and then exposed to ultraviolet irradiation at 185 nm. The charge states were determined using a tandem differential mobility analyzer system, and the results revealed that there was no significant dependence of charging probability upon mobility diameter between 4 and 60 nm ( $1.55 \pm 0.26$  in positive elementary charge), probably because of the agglomerated nature of the particles. The ionized particles could be deposited to form nanoscale island patterns on a substrate without the use of templates.



## INTRODUCTION

Aerosol particles can be electrically charged in numerous ways, including heating or exposure to an electromagnetic field, with the number of elementary charges on a particle dependent upon the charging mechanism. Electrostatic interactions between particles can be either attractive or repulsive depending upon charge. The charge magnitude and polarity can be controlled by adjusting both the particle concentration and the concentration of surrounding ions.<sup>1</sup> Accurate information on the magnitude and distribution of the particle charge is essential for examining the electrostatic effects in many fields of science and technology, e.g., atmospheric physics, aerosol-phase-based material synthesis, contamination control, etc.<sup>2–5</sup>

Incorporation of nanoparticles in quantum devices, field emission displays, single-electron transistors, and data storage devices requires precise patterning of well-separated nanoparticles on desired substrates.<sup>6</sup> Presently, lithography is the major workhorse for generating nanoparticle patterns. Nonetheless, lithographic techniques are fairly expensive, complicated, and time-consuming. Significant advances have been made in manipulating, delivering, and assembling a wide range of nanomaterials in predefined architectures and patterns. The realization of these architectures has largely depended upon the development of nanolithographic techniques.<sup>7</sup> A challenge today can be found in the design of aerosol systems that combine aerosol nanoparticle synthesis with local area deposition on foreign substrates for nanodevice applications.<sup>8</sup> Previous reports discussed a method for depositing freshly generated aerosol nanoparticles on a substrate using an electrostatically focused attraction between charged nanoparticles and substrates.<sup>9–12</sup>

Gold nanoparticles are used for a variety of industrial and commercial applications in biology, catalysis, and other nanotechnologies.<sup>13,14</sup> Even though wet chemical methods to prepare gold nanoparticles are the methods most commonly employed, the use of solvents can lead to particle contamination and unwanted surface modification because of

solvent-derived impurities.<sup>15</sup> Gas-phase approaches for producing gold nanoparticles offer distinct advantages. In particular, these approaches, which include inert gas condensation,<sup>16</sup> flame synthesis,<sup>17</sup> glowing wire generation,<sup>18</sup> and others, offer the possibility of green synthesis. This report concerns the generation of gold particles produced in an atmospheric pressure, non-equilibrium discharge,<sup>19</sup> which has been employed previously to produce gold nanoparticles.<sup>20–23</sup>

Direct irradiation and photoionization can be used to generate high number concentrations of positive and negative gaseous ions.<sup>24</sup> Photoionization has been considered as an effective means of positive charging of nanoparticles in plasma syntheses.<sup>25</sup> In the present work, direct photoionization was employed to create positively charged gold aerosol particles. The charge distributions of nanosized aerosol gold agglomerates passing through an ultraviolet (UV) irradiation chamber were determined. A tandem differential mobility analyzer (TDMA)<sup>26</sup> was employed to measure the positive elementary charges of gold agglomerates. The photoionized gold particles were then manipulated to produce nanoscale islands on a silicon wafer substrate without using lithographical masks or templates, which is different from conventional methods.

## METHODS

Figure 1 shows a schematic diagram of the process for the photoionization of aerosol gold agglomerates and the deposition of the ionized particles on a silicon wafer substrate. A spark discharge reactor was used to produce aerosol gold nanoparticles. The spark channels were formed between two identical gold rods (diameter of 3 mm and length of 100 mm, AU-172561, Nilaco, Japan) inside a reactor (volume of 42.8 cm<sup>3</sup>) under a pure nitrogen environment (purity of 99.9999%) at standard temperature and pressure conditions. The TDMA system consisted of two nano differential electrical mobility analyzers (NDMA, 3085, TSI, Shoreview, MN), NDMA 1 and NDMA

Received: April 20, 2014

Revised: July 3, 2014

Published: July 4, 2014



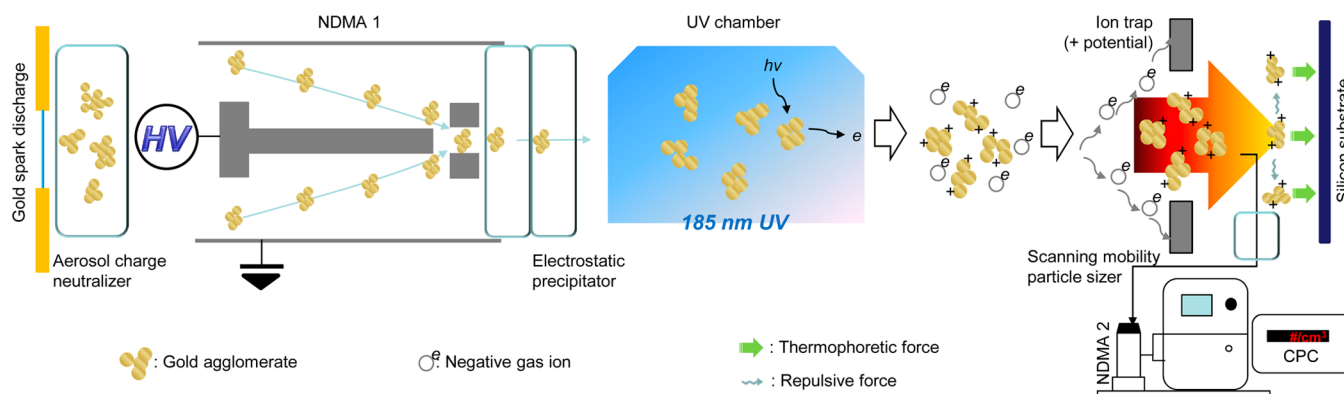


**Figure 1.** Schematic of photoionization of nanosized aerosol gold agglomerates and their deposition to produce nanoscale islands.

2, and a condensation particle counter (CPC, 3776, TSI, Shoreview, MN). NDMA 1 and NDMA 2 were placed before and after a glass chamber, which contained an UV lamp (3SC-9-A0, UVP, Cambridge, U.K.) operating a wavelength of 185 nm. NDMA 1 functioned as an electrostatic particle classifying system, which was operated at a chosen fixed voltage provided by a direct current power supply (205B, Bertan, Hauppauge, NY) to extract the particles of equivalent electrical mobility. The particles exiting NDMA 1 (all with equivalent electrical mobility) passed through a serial system consisting of an aerosol charge neutralizer (4810, HCT, Icheon, South Korea) and a cylindrical electrostatic precipitator to form uncharged monodisperse particles. The particles were finally directed into the UV chamber and irradiated at an intensity of  $0.14 \text{ J m}^{-2} \text{ s}^{-1}$ , as estimated from the UV lamp specification and gas flow rate. To prevent charge neutralization of photoionized particles by coexisting negative ions, an ion trap was employed to collect the negative ions from the UV chamber. The particle loss to the trap was less than 2% under the maximum negative ion current (measured by Keithley 6517B electrometer) when the ion trap voltage was selected as +38 V. Upon leaving the trap, the aerosol was directed to NDMA 2, which was used to measure the charge distribution corresponding to the initially selected mobility diameter. To fabricate nanoscale islands, the temperature of the size-classified, photoionized, particle-laden flow was maintained at  $19^\circ\text{C}$  with a tube heater, and the temperature of the silicon wafer substrate was maintained at  $-16^\circ\text{C}$ , thereby enhancing deposition of the particles onto the substrate via thermophoresis. Site-selective deposition of aerosol particles using electric fields was achieved for forming copper seeds for silver micropattern deposition in a previous study.<sup>27</sup> Thermophoretic particle motion is usually described by the thermophoretic particle velocity

$$v_{\text{th}} = -K_{\text{th}} \frac{\mu_g dT}{\rho_g T_p} \quad (1)$$

where  $dT$  represents the temperature gradient in the vicinity of the particle,  $\mu_g$  is the gas dynamic viscosity,  $T_p$  is the particle temperature, and  $\rho_g$  is the gas density, and  $K_{\text{th}}$  is the thermophoretic coefficient, which increases with decreasing of the particle size. Temperatures were measured by an infrared thermometer (42545, Extech, Nashua, NH) and maintained by a resistive heater and a Peltier cooler.

## RESULTS AND DISCUSSION

Figure 2 summarizes the size distributions of the particles formed by spark discharge between the gold rods. The geometric mean diameter (GMD, mobility equivalent diameter), geometric standard deviation (GSD), and total number concentration (TNC) of the spark-produced gold particles were 32.7 nm, 1.53, and  $2.08 \times 10^7 \text{ particles cm}^{-3}$ , respectively. This implies that the size distribution may be suitable for fabrication of gold islands with sizes between 10 and 100 nm in mobility diameter. In comparison to a previous study,<sup>20</sup> GSD is

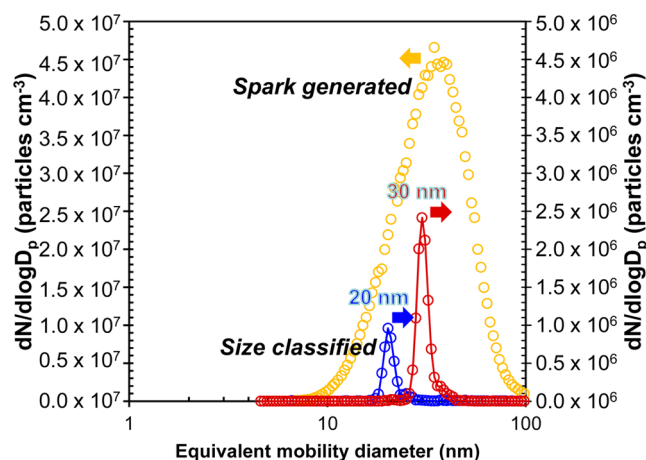


**Figure 2.** Size distribution of aerosol gold particles from a spark discharge. Distributions of size-classified particles with equivalent mobility diameters of 20 and 30 nm are also displayed.

larger than that of the previous work because of the larger TNC value (from different uses of capacitance of 1 nF versus 10 nF, the previous work), although GMD is smaller than was previously measured. The analogous results for the 20 nm classified gold particles were 20.2 nm, 1.08, and  $7.57 \times 10^4 \text{ particles cm}^{-3}$ , respectively, and the analogous results for the 30 nm classified particles were 30.1 nm, 1.09, and  $1.98 \times 10^5 \text{ particles cm}^{-3}$ , respectively. The size-classified particles showed substantially narrower GSD values than the non-classified case. Hence, this is a method for producing a uniform nanoparticle source for creating nanoscale islands on a silicon wafer substrate.

Figure 3 shows representative high- and low-magnification transmission electron microscopy (TEM, CM-100, FEI/Philips, Hillsboro, OR) images of size-classified gold particles. Selected mobility diameters were 20 and 30 nm. Specimens were prepared for examination by TEM using direct electrostatic aerosol sampling at a sampling flow of  $1.0 \text{ L min}^{-1}$  and an operating voltage of 5 kV using a nano particle collector (NPC-10, HCT, Icheon, South Korea). This electrostatic sampler was designed to couple directly downstream of NDMA to capture size-classified particles onto TEM grids or non-conductive substrates. Both images (panels a and b of Figure 3) establish that the gold particles were agglomerates of several primary particles, with primary particles of  $\sim 4 \text{ nm}$  diameter. The size of the primary particles is consistent with a previous report (3.5 nm).<sup>20</sup> Gaps between primary particles might have originated

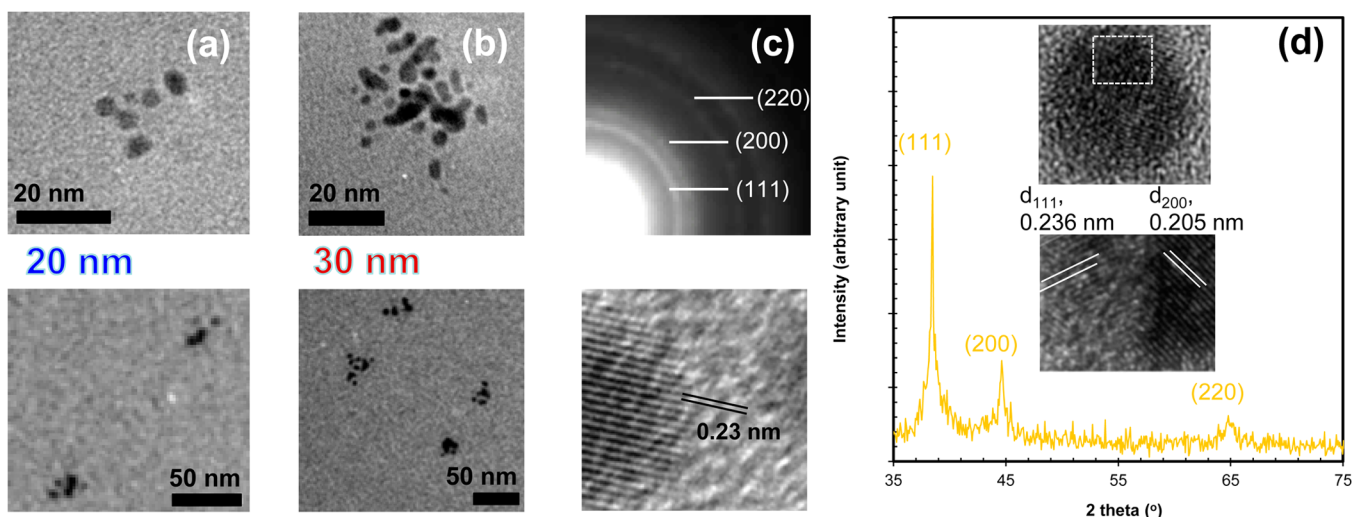


**Figure 3.** TEM images of gold particles classified by size as (a) 20 nm and (b) 30 nm, (c) ED pattern and microstructure of gold particles, and (d) XRD profile with high-magnification TEM images of gold lattice indices (111) and (200).

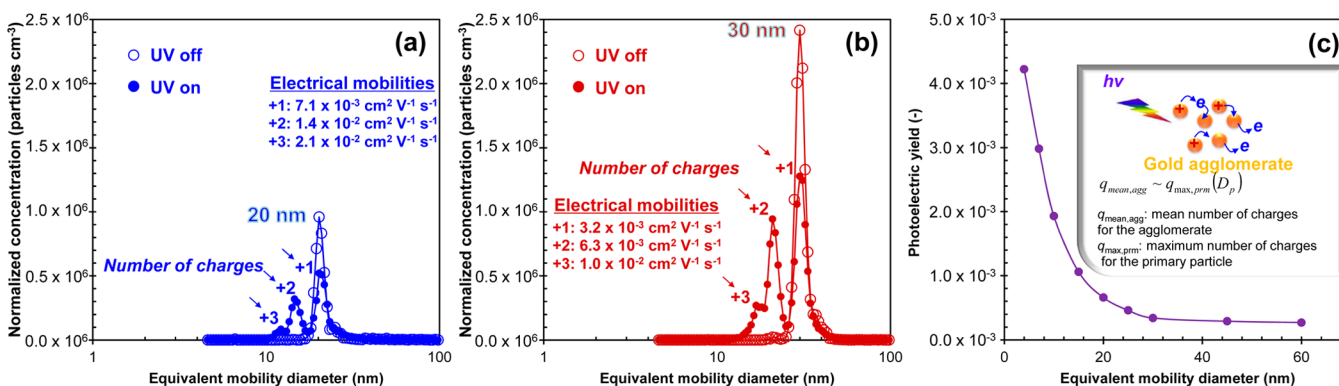


**Figure 4.** Results for photoionization of gold agglomerates. Charge distributions of UV-treated (a) 20 nm and (b) 30 nm gold particles. (c) Photoelectric yields of gold particles ranging from 4 to 60 nm in equivalent mobility diameter. The inset in panel c displays a phenomenon of charge-discharge by the electron movement within a network of primary gold particles in an agglomerate.

from impaction between the gold agglomerates and the silicon wafer substrate. Kinetic energy values of the 20 and 30 nm sized gold agglomerates directing onto the silicon wafer by thermophoresis are  $1.98 \times 10^{-20}$  and  $6.68 \times 10^{-20}$  J, respectively, which are significantly smaller than those ( $> 5 \times 10^{-18}$  J) in previous reports for initiating fragmentation of tightly bonded aerosol agglomerates (very small gaps between the primary particles).<sup>28,29</sup> This implies that the agglomerates in the aerosol state consisted of weakly cohering primary gold particles, which could easily fragment upon thermophoretic deposition. In addition, agglomeration in the aerosol state has probably performed between positively charged gold primary particles because most spark-produced metallic particles were naturally positively charged because of energetic electron bombardment,<sup>30</sup> resulting in weak agglomerate architectures. Figure 3c shows the electron diffraction (ED) obtained of the sample used for TEM analysis. The pattern has a sharp diffraction line showing the (111) reflection and weak diffraction lines showing the (200) and (220) reflections of the face-centered cubic lattice for metallic gold. The ratio of peak intensity (111)/(200) was 3.1 from X-ray diffraction (XRD, RINT-2100, Rigaku, Japan) measurements (Figure 3d) and was smaller than those of anisotropic particles (e.g., rod and dendrite).<sup>31</sup> This indicates the presence of a rather

spherical morphology of gold. A representative high-resolution image (also shown in Figure 3c) with lattice fringes having a spacing of 0.23 nm (cf. 0.2355 nm for bulk gold) further confirmed a growth of gold particles with the (111) plane. Other lattice indices [e.g., (200)] could also be observed at other primary gold particles depending upon their geometry under the electron beam, as shown in Figure 3d. The average particle size estimated from XRD line broadening of the (111) peak (Figure 3d), according to Scherrer's formula, was 3.3 nm, and this is consistent with that obtained by TEM.

Figure 4 shows charge distributions of photoionized gold particles. Different peaks appearing in panels a and b of Figure 4 correspond to the different number of charges on the particles. The number of elementary charges  $q$  of the photoionized particles was estimated using the following equation:

$$q = \frac{Z_{\text{p,NDMA } 2}}{Z_{\text{p,NDMA } 1}} \quad (2)$$

where  $Z_{\text{p,NDMA } 1}$  and  $Z_{\text{p,NDMA } 2}$  are the electrical mobilities measured by NDMA 1 and NDMA 2, respectively. The results reveal that the UV irradiation induced positive charges on the particles and that the highest number of elementary charges



(on the basis of  $>10^3$  particles  $\text{cm}^{-3}$ ) was 3 for both size-classified cases.

$$q_{\text{mean}} = \frac{I}{C_p Q e} \quad (3)$$

$$Y(h\nu) = \left( \frac{4q_{\text{mean}} h\nu}{\pi D_p^2 I_{\text{UV}} t} \right) \left( \frac{\Phi_{\infty}^2 - \Phi_{\infty}}{\Phi^2 - \Phi} \right) \quad (4)$$

$$q_{\text{max}}(D_p) = \frac{2\pi\epsilon_0}{e^2} (h\nu - \Phi_{\infty}) D_p - \frac{3}{8} \quad (5)$$

The mean number of charges  $q_{\text{mean}}$  for the 20 and 30 nm classified cases was 1.49 and 1.61, respectively, which is consistent with results from other measurements [refer to eq 3, where  $I$  is the current,  $C_p$  is the number concentration of particles,  $Q$  is the sampling flow rate, and  $e$  is the elementary unit of charge ( $1.6 \times 10^{-19}$  C)] using an aerosol electrometer (5.705, Grimm, Stuttgart, Germany). From the measurements using the electrometer, the photoelectric yield  $Y(h\nu)$  [refer to eq 4, where  $h\nu$  is the photon energy (6.22 eV),  $D_p$  is the particle size,  $I_{\text{UV}}$  is the irradiation intensity,  $t$  is the irradiation time, and  $\Phi_{\infty}$  and  $\Phi$  are the work function (5.31 eV) and phototreshold, respectively],<sup>32</sup> defined as the number of electrons ejected per photons absorbed, can be derived, as shown in Figure 4c. The data points in Figure 4c are derived from measurements of the mean number of charges using an aerosol electrometer for size-classified, photoionized particles. The measurements were performed in triplicate, and the results were reported as means. The results were comparable to previous reports for measurements of the yields ( $\sim 10^{-3}$ ) of gold.<sup>33,34</sup> On the other hand, the mean number of charges was  $1.55 \pm 0.26$  for the employed particle sizes, although the theoretical maximum charges [refer to eq 5, where  $\epsilon_0$  is the permittivity of the vacuum ( $8.85 \times 10^{-12}$  C<sup>2</sup> N<sup>-1</sup> m<sup>-2</sup>)] of the particles linearly increases between 1.6 and 29.0. The measured charges coincided with the theoretical value for 4 nm, a size that is consistent with the mean diameter of the primary particles in gold agglomerates. Some photogenerated electrons could be confined within a network of primary gold particles in an agglomerate, and this may induce repetitive charge–discharge of the primary particles (refer to the inset of Figure 4c). The result would be suppressed saturation of particle photoionization, resulting in a lower degree of charge compared to the theoretical values.

Islands of nanoparticles on foreign substrates are of great interest in plasmonic devices and in trace chemical detectors based on surface-enhanced Raman scattering.<sup>35</sup> Figure 5 shows scanning electron microscopy (SEM, NOVA nanoSEM, FEI, Hillsboro, OR) images of the thermophoretically deposited

photoionized particles on silicon wafer substrates. A schematic diagram of the apparatus used to produce the nanoscale islands is shown in Figure 1. The method involves the photoionization of aerosol gold nanoparticles via UV irradiation and subsequent thermophoretic deposition on a silicon substrate [N type (100), with resistivity from  $10^{-2}$  to  $10^{-3}$   $\Omega$  cm]. The temperature of the particle-laden flow was maintained at 19 °C using a tube heater, and the temperature of the silicon substrate was maintained at  $-16$  °C, thereby enhancing deposition of the particles onto the substrate via thermophoresis.<sup>36</sup> The SEM images reveal that the agglomerates (mobility classified at 20 and 30 nm) are spread out over the entire surface with gaps between agglomerates, because of the electrostatic repulsion before deposition.<sup>30,37,38</sup> Relocation of the particles by 20 nm (or 30 nm) would require an external force (i.e., detachment force,  $F_{\text{det}}$ ) to affect particle motion on the substrate. Brownian forces ( $F_{\text{Brown}}$ )<sup>39</sup> and van der Waals attraction ( $F_{\text{vdW}}$ )<sup>40</sup> were smaller ( $\sim 10^{-12}$  N) than the  $F_{\text{det}}$  [ $\sim 10^{-11}$  N, van der Waals force between the particle and substrate ( $F'_{\text{vdW}}$ ),<sup>41</sup> capillary force ( $F_{\text{cap}}$ ),<sup>41</sup> and thermophoretic force ( $F_T$ )].<sup>42</sup> Even though the particles lose charge upon deposition, their location on the substrate barely changes. Photoionization of the size-classified gold particles shows that the repulsive interaction because of the particle charges acted as a potential barrier, which suppressed further agglomeration of gold nearly completely during deposition, resulting in the formation of nanoscale islands on a silicon wafer substrate without the use of templates. Straight-line distances between the centers of the deposited particles for the 20 and 30 nm size-classified cases were  $69 \pm 9.6$  and  $71 \pm 9.8$  nm, respectively. This implies that there are no significant differences between the distances because of a narrow variation of the charge amount ( $\sim 1.55$  in mean number of charge). Values of the measured mean number of charges (1.49 for 20 nm and 1.61 for 30 nm) are smaller than those of theoretically estimated values (3.71 for 20 nm and 7.89 for 30 nm for single-body spherical particles). This implies that controllable ranges between gold agglomerates may not be broad enough to fabricate a variety of gold island configurations. To increase the distance range, the agglomerated gold particles may often need to be treated with high temperatures<sup>43,44</sup> or surface functionalization with polar components<sup>45,46</sup> to form broader ranges for the charges on a particle surface.

## CONCLUSION

For the first time, the photoionization was used to create positively charged nanosized aerosol gold particles. The particles were then employed to form nanoscale islands of gold agglomerates on a silicon wafer substrate, without the use of templates and any wet chemical steps. This method may provide a practical and relevant strategy for the controllable fabrication of various metal island films or nanoscale island arrays and also provide new opportunities to construct future optoelectronic and sensing devices. Thermal curing or surface functionalization with polar components may often require forming broader ranges for the charges on a particle surface, which would be a viable option for fabricating a variety of nanoscale metal islands on a foreign substrate.

## AUTHOR INFORMATION

### Corresponding Author

\*Telephone: +1-765-494-1730. Fax: +1-765-494-1736. E-mail: jtrob@purdue.edu.

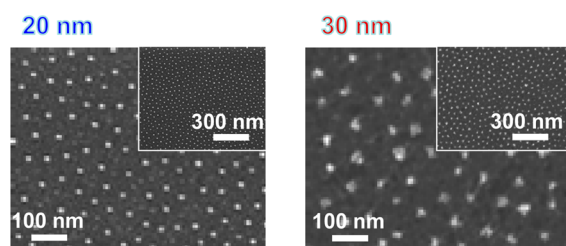


**Figure 5.** SEM images for the deposition of photoionized gold particles (20 and 30 nm) on silicon wafer substrates.

## Notes

The authors declare no competing financial interest.

## ■ ACKNOWLEDGMENTS

This work was partially supported by National Science Foundation (NSF) Grant CHE-0924431.

## ■ REFERENCES

- (1) Horenstein, M. N. Electrostatics and nanoparticles: What's the same, what's different? *J. Electrostat.* **2009**, *67*, 384–393.
- (2) Borra, J.-P. Nucleation and aerosol processing in atmospheric pressure electrical discharges: Powders production, coatings and filtration. *J. Phys. D: Appl. Phys.* **2006**, *39*, R19–R54.
- (3) Tsai, C.-J.; Lin, J.-S.; Deshpande, C. G.; Liu, L.-C. Electrostatic charge measurement and charge neutralization of fine aerosol particles during the generation process. *Part. Part. Syst. Charact.* **2005**, *22*, 293–298.
- (4) Forsyth, B.; Liu, B. Y. H.; Romy, F. J. Particle charge distribution measurement for commonly generated laboratory aerosols. *Aerosol Sci. Technol.* **1998**, *28*, 489–501.
- (5) Maisels, A.; Jordan, F.; Fissan, H. On the effect of charge recombination on the aerosol charge distribution in photocharging systems. *J. Aerosol Sci.* **2003**, *34*, 117–132.
- (6) Lenggoro, I. W.; Lee, H. M.; Okuyama, K. Nanoparticle assembly on patterned “plus/minus” surfaces from electrospray of colloidal dispersion. *J. Colloid Interface Sci.* **2006**, *303*, 124–130.
- (7) Chen, J.-K.; Qui, J.-Q. Patterned 3D assembly of Au nanoparticle on silicon substrate by colloid lithography. *J. Nanopart. Res.* **2012**, *14*, 942–956.
- (8) Lin, E.-C.; Cole, J. J.; Jacobs, H. O. Gas phase electrodeposition: A programmable multimaterial deposition method for combinatorial nanostructured device discovery. *Nano Lett.* **2010**, *10*, 4494–4500.
- (9) Kim, H.; Kim, J.; Yang, H.; Suh, J.; Kim, T.; Han, B.; Kim, S.; Kim, D.; Pikhitsa, P. V.; Choi, M. Parallel patterning of nanoparticles via electrodynamic focusing of charged aerosols. *Nat. Nanotechnol.* **2006**, *1*, 117–121.
- (10) You, S.; Han, K.; Kim, H.; Lee, H.; Woo, C. G.; Jeong, C.; Nam, W.; Choi, M. High-resolution, parallel patterning of nanoparticles via an ion-induced focusing mask. *Small* **2010**, *6*, 2146–2152.
- (11) Lee, H.; You, S.; Pikhitsa, P. V.; Kim, J.; Kwon, S.; Woo, C. G.; Choi, M. Three-dimensional assembly of nanoparticles from charged aerosols. *Nano Lett.* **2011**, *11*, 119–124.
- (12) Lim, K.; Lee, J.-R.; Lee, H.; Pikhitsa, P. V.; You, S.; Woo, C. G.; Kim, P.; Suh, K. Y.; Choi, M. Nanoxerography utilizing bipolar charge patterns. *Appl. Phys. Lett.* **2012**, *101*, 203106.
- (13) Boisselier, E.; Astruc, D. Gold nanoparticles in nanomedicine: Preparations, imaging, diagnostics, therapies and toxicity. *Chem. Soc. Rev.* **2009**, *38*, 1759–1782.
- (14) Daniel, M.-C.; Astruc, D. Gold nanoparticles: Assembly, supramolecular chemistry, quantum-size-related properties, and applications toward biology, catalysis, and nanotechnology. *Chem. Rev.* **2004**, *104*, 293–346.
- (15) Boies, A.; Lei, P.; Calder, S.; Shin, W. G.; Girshick, S. L. Hot-wire synthesis of gold nanoparticles. *Aerosol Sci. Technol.* **2011**, *45*, 654–663.
- (16) Heurlin, M.; Magnusson, M. H.; Lindgren, D.; Ek, M.; Wallenberg, L. R.; Deppert, K.; Samuelson, L. Continuous gas-phase synthesis of nanowires with tunable properties. *Nature* **2012**, *492*, 90–94.
- (17) Mädler, L.; Stark, W. J.; Pratsinis, S. E. Simultaneous deposition of gold nanoparticles during flame synthesis of titania and silica. *J. Mater. Res.* **2003**, *18*, 115–120.
- (18) Chan, K. W.; Rahman, S. A.; Aspanut, Z. Effect of rapid thermal annealing time on Au/SiO<sub>x</sub> film prepared by hot wire assisted plasma enhanced chemical vapour deposition technique. *Mater. Chem. Phys.* **2013**, *140*, 37–41.
- (19) Ostrikov, K.; Neyts, E. C.; Meeyappan, M. Plasma nanoscience: From nano-solids in plasmas to nano-plasmas in solids. *Adv. Phys.* **2013**, *62*, 113–224.
- (20) Byeon, J. H.; Park, J. H.; Hwang, J. Spark generation of monometallic and bimetallic aerosol nanoparticles. *J. Aerosol Sci.* **2008**, *39*, 888–896.
- (21) Byeon, J. H.; Kim, J.-W. Carbon fiber coating with silver using intervening Au/Pd nanoparticle films produced using a spark discharge. *Thin Solid Films* **2010**, *519*, 700–705.
- (22) Byeon, J. H.; Roberts, J. T. Aerosol-based fabrication of biocompatible organic–inorganic nanocomposites. *ACS Appl. Mater. Interfaces* **2012**, *4*, 2693–2698.
- (23) Byeon, J. H.; Roberts, J. T. Aerosol based fabrication of thiol-capped gold nanoparticles and their application for gene transfection. *Chem. Mater.* **2012**, *24*, 3544–3549.
- (24) Han, B.; Shimada, M.; Choi, M.; Okuyama, K. Unipolar charging of nanosized aerosol particles using soft X-ray photoionization. *Aerosol Sci. Technol.* **2003**, *37*, 330–341.
- (25) Ostrikov, K. N.; Yu, M. Y.; Stenflo, L. Surface waves in strongly irradiated dusty plasmas. *Phys. Rev. E: Stat. Phys., Plasmas, Fluids, Relat. Interdiscip. Top.* **2000**, *61*, 782–787.
- (26) Shimada, M.; Okuyama, K.; Inoue, Y.; Adachi, M.; Fujii, T. Removal of airborne particles by a device using UV/photoelectron method under reduced pressure conditions. *J. Aerosol Sci.* **1999**, *30*, 341–353.
- (27) Byeon, J. H.; Kim, Y.-W. Aerosol copper initiated core–shell nanoparticle synthesis and micropatterning. *New J. Chem.* **2012**, *36*, 2184–2187.
- (28) Byeon, J. H.; Ji, J. H.; Park, J. H.; Yoon, K. Y.; Hwang, J. Charge distributions of aerosol dioctyl sebacate particles charged in a dielectric barrier discharger. *J. Aerosol Sci.* **2008**, *39*, 460–466.
- (29) Rothenbacher, S.; Messerer, A.; Kasper, G. Fragmentation and bond strength of airborne diesel soot agglomerates. *Part. Fibre Toxicol.* **2008**, *5*, 9.
- (30) Froeschke, S.; Kohler, S.; Weber, A. P.; Kasper, G. Impact fragmentation of nanoparticle agglomerates. *J. Aerosol Sci.* **2003**, *34*, 275–287.
- (31) Byeon, J. H.; Kim, Y.-W. Chitosan-conjugated dendritic Ag nanopowders for photothermal therapy applications. *ACS Macro Lett.* **2014**, *3*, 205–210.
- (32) Byeon, J. H.; Kim, J.-W. Fabrication of a pure, uniform electroless silver film using ultrafine silver aerosol particles. *Langmuir* **2010**, *26*, 11928–11933.
- (33) Maisels, A.; Jordan, F.; Fissan, H. Dynamics of the aerosol particle photocharging process. *J. Appl. Phys.* **2002**, *91*, 3377–3383.
- (34) Jackson, R. S.; Matsunaga, F. M.; Watanabe, K. *Some Intensity Measurements in the Vacuum Ultraviolet*; National Aeronautics and Space Administration (NASA): Washington, D.C., 1964.
- (35) Schmidt-Ott, A.; Schurtenberger, P.; Siegmund, H. C. Enormous yield of photoelectrons from small particles. *Phys. Rev. Lett.* **1980**, *45*, 1284–1287.
- (36) Rutkevych, R. P.; Ostrikov, K.; Xu, S.; Vladimirov, S. V. Thermophoretic control of building units in the plasma-assisted deposition of nanostructured carbon films. *J. Appl. Phys.* **2004**, *96*, 4421–4428.
- (37) Byeon, J. H.; Roberts, J. T. Silver deposition on a polymer substrate catalyzed by singly charged monodisperse copper nanoparticles. *ACS Appl. Mater. Interfaces* **2012**, *4*, 2515–2520.
- (38) Krinke, T. J.; Deppert, K.; Magnusson, M. H.; Schmidt, F.; Fissan, H. Microscopic aspects of the deposition of nanoparticles from the gas phase. *J. Aerosol Sci.* **2002**, *33*, 1341–1359.
- (39) Wang, X.; Gidwani, A.; Girshick, S. L.; McMurtry, P. H. Aerodynamic focusing of nanoparticles: II. Numerical simulation of particle motion through aerodynamic lenses. *Aerosol Sci. Technol.* **2005**, *39*, 624–636.
- (40) Feng, Y.; Lin, J.-Z. The collision efficiency of spherical dioctyl phthalate aerosol particles in the Brownian coagulation. *Chin. Phys. B* **2008**, *17*, 4547–4553.

- (41) Park, H.-S.; Choa, S.-H.; Hwang, J. Effect of lubricant characteristics on particle adhesion and removal in a magnetic hard disk surface. *J. Info. Storage Proc. Syst.* **2001**, 3, 213–220.
- (42) Setyawan, H.; Shimada, M.; Ohtsuka, K.; Okuyama, K. Visualization and numerical simulation of fine particle transport in a low-pressure parallel plate chemical vapor deposition reactor. *Chem. Eng. Sci.* **2002**, 57, 497–506.
- (43) Nakaso, K.; Shimada, M.; Okuyama, K.; Deppert, K. Evaluation of the change in the morphology of gold nanoparticles during sintering. *J. Aerosol Sci.* **2002**, 33, 1061–1074.
- (44) Svensson, C. R.; Messing, M. E.; Lundqvist, M.; Schollin, A.; Deppert, K.; Pagels, J. H.; Rissler, J.; Cedervall, T. Direct deposition of gas phase generated aerosol gold nanoparticles into biological fluids—Corona formation and particle size shifts. *PLoS One* **2013**, 8, No. e74702.
- (45) Calder, S.; Boies, A.; Lei, P.; Girshick, S.; Roberts, J. Photo-assisted hydrosilylation of silicon nanoparticles: Dependence of particle size on grafting chemistry. *Chem. Mater.* **2011**, 23, 2917–2921.
- (46) Chiang, C.-T.; Roberts, J. T. Surface functionalization of zinc oxide nanoparticles: An investigation in the aerosol state. *Chem. Mater.* **2011**, 23, 5237–5242.